



## Studying of physicochemical properties of coumarin based nano-complexes for biomedical applications

Walaa H. Mahmoud<sup>a</sup>, Mervat S. Mostafa<sup>\*b</sup>, M.M. Omar<sup>a</sup>, Gehad G. Mohamed<sup>a</sup>

<sup>a</sup> Chemistry Department, Faculty of Science, Cairo University, Giza, 12613 Egypt

<sup>b</sup> Science and Technology Center of Excellence (STCE), Ministry of Military Production, Cairo, Egypt



CrossMark

### Abstract

Novel Schiff base ligand based on coumarin precursor was prepared by the condensation of 3-acetyl coumarin with 3-aminophenol. The newly synthesized Cr(III), Mn(II), Fe(III), Co(II), Ni(II), Cu(II), Zn(II), and Cd(II) complexes were characterized by elemental analysis, molar conductivity, spectroscopic techniques (IR, <sup>1</sup>H NMR, mass spectrometry, UV-Vis), and thermal analysis (TG/DTG) to predict their structures. The resulting data displays octahedral complexes with 1M:1L ratio. The IR confirmed that the ligand coordinated to the metal ions in tridentate mode with ONO coordination sites. The complexes decomposed with three to five steps within the temperature range 30-900 °C. Additionally, mass spectra of the ligand and its Cu(II) complex offer well matching data with calculated value. The molar conductivity values pointed out that the complexes were non-electrolytes. Molecular optimization of prepared compositions at DFT/LANL2DZ level, besides Molecular docking between Schiff base ligand (HL) and the receptors of breast cancer were executed. Additionally, antibacterial activity has been evaluated against *Streptococcus aureus* and *Escherichia coli*. Additionally, fungicidal activity was screened *in vitro* against *Aspergillus flavus* and *Candida albicans*, using the disc diffusion method. The [Co(HL)Cl<sub>2</sub>.H<sub>2</sub>O].4H<sub>2</sub>O complex exhibits the highest antimicrobial effect against *Streptococcus aureus* with inhibition area 17mm, while against *Escherichia coli* it records 14mm, and 12mm against *Candida albicans*. The [Mn(L)Cl<sub>2</sub>.H<sub>2</sub>O].4H<sub>2</sub>O complex shows the lowest IC<sub>50</sub> against human cancer (MCF-7 cells viability) with 22.2 µg/ml.

**Keywords:** coumarin Schiff base; spectroscopy; complexes; Molecular docking; Antimicrobial; anticancer; DFT and HF Computational; thermal analysis.

### 1. Introduction

Recently, healthcare has been becoming challenges including anticancer treatment and antimicrobial resistance (AMR) [1]. Various methods have been utilized for cancer treatment including surgery, chemotherapy, besides radiotherapy. Regarding AMR, microorganisms which exhibiting mutations against the medications are called “superbugs”, thus common drugs failed to treat such infections, additionally, designing new adjusted medications becomes an attractive field for controlling the threat of AMR [2-4]. Cisplatin was the starting seed in using inorganic chemistry for anti-cancer drug candidates. Transition metal based biocompatible complexes showed excellent bioactivity, while, first row of transition metals exhibit noticeable efficiency in relatively small quantities [5]. Recently, Schiff base complexes have a fast development in biomedical field, tailoring new compounds with morphological and physicochemical

properties proper to anticancer and antibacterial complications. Condensation of primary amine (NH<sub>2</sub>) with carbonyl group (C=O) forming Schiff bases with characteristic azomethine (-C=N-) function group with resemblance to compounds naturally exist in living organisms [6, 7]. Moreover, azomethine group belongs lone pair of electrons in sp<sup>2</sup> hybridized orbital of nitrogen atom that offer bonding capability with metals, forming coordination compounds, thus, chemical and biological properties could be originated from ligand activity [8, 9]. Schiff bases obtained from amine and heterocyclic ring have been found an interest because of their pharmacological properties [10, 11]. Behavior of Schiff bases depend on its row materials [10]. Coumarin is one of the materials that able to be a root of Schiff bases, while coumarin consists of benzene structure attached to a pyrone ring. The latter is naturally existing organic material that extracted from Tonka tree beans [12]. Transition metal complexes of symmetrical and asymmetrical Schiff

\*Corresponding author e-mail: [mervat\\_s.mostfa@yahoo.com](mailto:mervat_s.mostfa@yahoo.com); (Mervat S. Mostafa).

Receive Date: 04 February 2021, Revise Date: 24 February 2021, Accept Date: 03 March 2021

DOI: 10.21608/EJCHEM.2021.61403.3322

©2021 National Information and Documentation Center (NIDOC)

bases have played a significant role in the field of coordination, inorganic and bioinorganic chemistry as models for biological, analytical and industrial applications [13]. Coumarins showed excellent antibiotics and fungicides effectiveness [14]. Furthermore, it recommended for diverse pharmaceutical agents such as anticoagulant, antibacterial, antiviral and anti-tumor [15] and plant regulating activities [16]. Coumarin's cytotoxic action encourages researchers to intensive investigation to obtain new antitumor agents. Further, Coumarins are effective not only for treatment of cancer, but also to treat the side effects caused by radiotherapy. Coumarins are very clear in the treatment of tumor and is used in the treatment of prostate cancer, renal cell carcinoma and leukemia. [17]. Many coumarin compounds, after some suitable structural modification can be used as drugs. Chelating ability of coumarin derivatives have been studied to suggest their use as chelating agents [16]. Moreover, 3-aminophenol is a second precursor in Schiff-base ligand preparation. The later have two different applicable donating electronegative atoms O and N able to coordinating transition metals [18]. Besides, 3-aminophenol showed biological and antibacterial activities.

Transition metals have special biological features [18, 19]. Thus, metal complexes based Schiff base have been exhibit different mechanism(s) of action from platinum drugs, while complexes reacted with DNA causing cleavage besides reactive oxygen species (ROS) are formed which lead to cell mortality [20]. For instance, iron (II) chelators are Often utilized as antitumor drug, that it enhance oxidative destruction in DNA, thus cause mortality to cancer cells [21]. Recent, researches have been exhibited Fe-complexes potential as anticancer agents by altered mechanisms [22, 23]. Moreover, copper has been considered as a vital biological element in human body, additionally copper complexes display excellent biological activity in biological applications [24, 25]. Copper species belong higher anticancer effectiveness besides lower toxicity than platinum medications, in addition to, it could overcome Cisplatin acquired resistance [26].

In this study, new Schiff base ligand was synthesized by coupling 3-acetylcoumarin with 3-aminophenol. Metal complexes based on prepared Schiff base were an efficient route with Cr(III), Mn(II), Fe(III), Co(II), Ni(II), Cu(II) and Zn(II) ions. Additionally, structural, morphological, and thermal properties are executed. Moreover, biological effectiveness of coordinating metal (II/III) complexes has been evaluated, aiming to investigate the antibacterial and anticancer activity of new biocompatible materials, more natural, with small quantities. Optimum geometric molecular structures

have been performed at DFT/ LANL2DZ level. Molecular docking studies were performed in order to evaluate the mode of bonding between the compounds under investigation and the crystal structure of the prepared ligand.

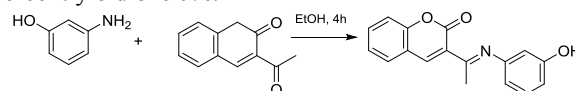
## Experimental

### 2.1. Materials and reagents

The precursors 3-acetylcoumarin, 3-amino-phenol,  $\text{CoCl}_2 \cdot 6\text{H}_2\text{O}$ ,  $\text{NiCl}_2 \cdot 6\text{H}_2\text{O}$ ,  $\text{MnCl}_2 \cdot 2\text{H}_2\text{O}$ ,  $\text{CdCl}_2$ ,  $\text{CuCl}_2 \cdot 2\text{H}_2\text{O}$ ,  $\text{ZnCl}_2$ ,  $\text{CrCl}_3 \cdot 6\text{H}_2\text{O}$  and  $\text{FeCl}_3 \cdot 6\text{H}_2\text{O}$  were provided from Sigma. Organic solvents such as ethanol (90%), diethylether and dimethylformamide (DMF) were used. Bi-distilled water was usually used in all preparations.

### 2.2. Synthesis of Schiff base ligand

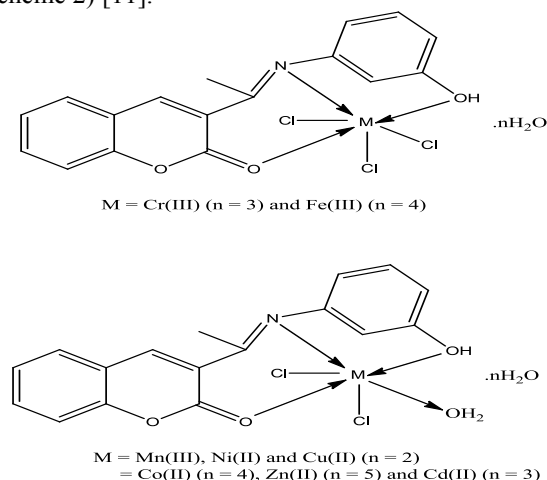
The Schiff base ligand was prepared by refluxing 3-acetylcoumarin (10 mmol, 1.89 g) with 3-aminophenol (10 mmol, 1.09 g) in ethanol solvent for 4 hrs. Throughout this step, brown color precipitate has been formed (Scheme 1). Then mixture solution has been air-conditioned at room temperature and the precipitate attained was filtered and air dried. The product was recrystallized from DMF-methanol (1:1 v/v) [11], with percent yield of 90%.



Scheme 1. Preparation of HL Schiff base ligand.

### 2.3. Synthesis of metal complexes

The Cr(III), Mn(II), Fe(III), Co(II), Ni(II), Cu(II), Cd(II) and Zn(II) complexes were prepared by a reaction of 1:1 molar mixture of hot ethanolic solution (60 °C) of the metal chloride (1 mmol) and the Schiff base ligand (1 mmol, 279 mg). The resulting solution was stirred under refluxing for 3 h, at this point the complexes precipitated. The resulting solution was cooled, filtered, purified by washing several times with diethyl ether then air dried (Scheme 2) [11].



Scheme 2. Structure of Schiff base metal complexes.

## 2.4. Instrumentations

Mass spectra were carried out using the EI technique at 70 eV using an MS-5988 GS- MS Hewlett-Packard instrument at the Micro analytical Center, National Center for Research, Egypt. Microanalyses of carbon, hydrogen and nitrogen were carried out at the Micro analytical Center, Cairo University, Egypt, using a CHNS-932 (LECO) Vario Elemental Analyzer. Analyses of the metals followed the dissolution of the solid complexes in concentrated HNO<sub>3</sub>, the metal content was carried out using inductively coupled plasma atomic absorption spectrometry (ICP-AES), Egyptian Petroleum Research Institute. Infrared spectra were recorded on 8001-PC FT-IR Shimadzu spectrophotometer using KBr pellets in the mid-infrared region 4000-400 Cm<sup>-1</sup>. <sup>1</sup>H NMR spectra, as a solution in DMSO-d<sub>6</sub>, were recorded on a 300 MHz Varian-Oxford Mercury at room temperature using TMS as an internal standard. UV-Vis spectra were carried out on UV mini-1240, UV-Vis spectrophotometer, Shimadzu. Solution of the Schiff base ligand and its metal complexes (1 \* 10<sup>-4</sup> M) were prepared for measuring UV-Vis spectra. A thermogravimetric analyzer (TGA Q500 TA INSTRUMENTS, USA). Approximately 1–20 mg of the sample, in an open aluminum pan, was heated in the TGA from room temperature to 900C at 10 °C/min under nitrogen purge. The scanning electron microscope (SEM) image of the complexes was recorded by using SEM Model Quanta 250 FEG (Field Emission Gun) attached with EDX unit (Energy Dispersive X-ray Analyses), with accelerating voltage 30 K.V., magnification 14X up to 1000000 and resolution for Gun. In, National Research Center, Egypt).

## 2.5. Computational investigation

The molecular structure of the Schiff base ligand was optimized by HF and DFT method with 3-21G basis set. The molecules were built with the Perkin Elmer ChemBio Draw and optimized using Perkin Elmer ChemBio3D software [27]. Quantum chemical parameters such as the highest occupied molecular orbital energy (E<sub>HOMO</sub>), the lowest unoccupied molecular orbital energy (E<sub>LUMO</sub>) and HOMO- LUMO energy gap (DE) for the investigated molecules were calculated.

## 2.6. The antimicrobial investigation

The antimicrobial activities were carried out at the Micro analytical Center, Cairo University, Egypt. The anticancer activity was performed at Al-Azhar University. The optical density (O.D.) of each well was measured spectrophotometric ally at 564 nm with an ELIZA micro plate reader (Meter tech. R 960, USA).

A filter paper disk (5 mm) was transferred into 250 mL flasks containing 20 mL of working volume of tested solution (100 mg/mL). All flasks were autoclaved for 20 min at 121° C. LB agar media surfaces were inoculated with investigated bacteria (Gram positive bacteria: *Staphylococcus aureus*; Gram negative bacteria: *Escherichia coli*; and one strain of fungi: *Aspergillus flavus* and *Candida albicans* by diffusion agar technique [28], then transferred to a saturated disk with a tested

solution in the center of a Petri dish (agar plates). All compounds were placed at four equidistant places at a distance of 2 cm from the center in the inoculated Petriplates. DMSO served as control. Finally, all Petri dishes were incubated at 25 °C for 48 h where clear or inhibition zones were detected around each disk. Control flask of the experiment was designed to perform under the same condition described previously for each microorganism but with dimethylformamide solution only and by subtracting the diameter of inhibition zone resulting with dimethylformamide from that obtained in each case, so antibacterial activity could be calculated [29],[16]. Ampicillin and Amphotericin were used as reference compounds for antibacterial and antifungal activities, respectively. All experiments were performed in triplicate, and data plotted were the mean value.

## 2.7. Anticancer study

Potential cytotoxicity of the compounds was tested using the method of Skehan and Storeng [29],[30]. Cells were plated in 96-multiwell plate (104 cells/well) for 24 h before treatment with the compounds to allow attachment of cells to the wall of the plate. Different concentrations of the compounds under investigation (0, 1, 2, 3.9, 7.8, 15.6, 31.25, 62.5, 125, 250 and 500 µg/mL) were added to the cell monolayer triplicate wells were prepared for each individual dose. The monolayer cells were incubated with the compounds for 48 h at 37 °C and in 5 % CO atmosphere. After 48 h, cells were fixed, washed, and stained with SRB stain. Excess stain was washed with acetic acid and attached stain was recovered with tris-EDTA buffer. The optical density (O.D.) of each well was measured spectrophotometrically at 564 nm with an ELISA microplate reader and the mean background absorbance was automatically subtracted and mean values of each drug concentration was calculated. The relation between surviving fraction and drug concentration is plotted to get the survival curve of Breast tumor cell line for each compound.

### Calculation

The percentage of cell survival was calculated as follows: Survival fraction = O.D. (treated cells)/O.D. (control cells)

The IC<sub>50</sub> values (the concentrations of symmetric Schiff base ligand or its complexes required to produce 50 % inhibition of cell growth) were calculated. The experiment was repeated three times for MCF7 cell line.

## 2.8. Solution of anticancer study

A fresh stock solution of 1\* 10<sup>-3</sup> M of complexes was prepared in the appropriate volume of ethanol (95 %). Dimethylsulphoxide (DMSO) (Sigma Chemical Co., St. Louis, MO, USA) was used in the cryopreservation of cells. RPMI-1640 medium (Sigma Chemical Co., St. Louis, MO, USA) was used. The medium was used to culture and maintain the human tumor cell line. The medium was supplied in a powder form. It was prepared as follows: 10.4 g medium was weighed, mixed with 2 g sodium bicarbonate, and distilled water was added to 1 L, and the mixture was shaken carefully until complete

dissolution. The medium was then sterilized by filtration in a Millipore bacterial filter (0.22  $\mu$ m). The prepared medium was kept in a refrigerator (4 °C) and checked at regular intervals for contamination. Before use, the medium was warmed at 37 °C in a water bath and supplemented with penicillin/streptomycin and FBS. Sodium bicarbonate (Sigma Chemical Co., St. Louis, MO, USA) was used for the preparation of RPMI-1640 medium. Isotonic Trypan blue solution (0.05 %; Sigma Chemical Co., St. Louis, MO, USA) was prepared in normal saline and was used for viability counting. Fetal bovine serum (10 %; FBS) (heat inactivated at 56°C for 30 min), 100 units/mL penicillin and 2 mg/mL streptomycin were supplied from Sigma Chemical Co., St. Louis, MO, USA and were used for the supplementation of RPMI-1640 medium prior to use. Trypsin (0.025 % (w/v); Sigma Chemical Co., St. Louis, MO, USA) was used for the harvesting of cells. Acetic acid (1 % (v/v); Sigma Chemical Co., St. Louis, MO, USA) was used for dissolving the unbound SRB dye. Sulphorhodamine-B (0.4 %; SRB) (Sigma Chemical Co., St. Louis, MO, USA) dissolved in 1% acetic acid was used as a protein dye. A stock solution of trichloroacetic acid (TCA, 50%, Sigma Chemical Co., St. Louis, MO, USA) was prepared and stored. Fifty microliters of the stock was added to 200  $\mu$ L RPMI-1640 medium/well to yield a final concentration of 10 % used for protein precipitation. One hundred percent Isopropanol and 70% ethanol were used. Tris base 10 mM (pH 10.5) was used for SRB dye solubilization. Tris base (121.1 g) was dissolved in 1000 mL of distilled water, and the pH was adjusted with HCl acid (2 M). [31]

#### Description of compounds

##### HL

Yield 99 %; brown solid, m.p 210 °C. Anal. Calcd. for  $C_{17}H_{13}NO_3$  (%): C, 73.12; H, 4.66; N, 5.018, Found (%): C, 73.02; H, 4.53; N, 4.99. Calcd. Mol.Wt. 279 (g/mole). IR ( $\nu$ ,  $cm^{-1}$ ): 3447br (OH), 1748sh (C=O coumarin) 1655sh (C=N), 1235m (C-O).  $^1H$  NMR ( $\delta$  ppm): 6.4-7.3 (m, 9H, ArH), 1.81 (t, 3H,  $CH_3$ ), 11.5 (s, 1H, phenolic OH) [32]. UV-Vis ( $\lambda$ , nm): 211( $\pi$ - $\pi^*$ ), 272 ( $\pi$ - $\pi^*$ ), and 331(n- $\pi^*$ ) transitions.

##### [Cr(HL)Cl<sub>3</sub>].3H<sub>2</sub>O

Yield 88%; reddish Brown solid, m.p >300 °C. Anal. Calcd. for  $Cr(C_{17}H_{13}NO_3Cl_3) \cdot 3H_2O$  (%): C, 41.51; H, 3.87; N, 2.85; M, 10.58. Found (%): C, 41.41; H, 3.83; N, 2.75; M, 10.53, Calcd. Mol.Wt. (g/mole) 491.5. IR ( $\nu$ ,  $cm^{-1}$ ): 3352br (OH), 1724sh (C=O coumarin), 1615m (C=N), 1234 Sh (C-O), 918w and 858w ( $H_2O$  coordinated water), 553s (M-O), 486s (M-N). UV-Vis ( $\lambda$ , nm): 208 ( $\pi$ - $\pi^*$ ), 269 ( $\pi$ - $\pi^*$ ), 327 (n- $\pi^*$ ) transitions.  $\Lambda_m$  ( $\Omega^{-1} mol^{-1} cm^2$ ): 41.3.

##### [Mn(HL)Cl<sub>2</sub>.H<sub>2</sub>O].2H<sub>2</sub>O

Yield 79%; faint brown solid, m.p >300 °C. Anal. Calcd. for  $Mn(C_{17}H_{13}NO_3Cl_2.H_2O) \cdot 2H_2O$  (%): C, 44.44; H, 4.14; N, 3.05; M, 11.98. Found (%): C, 44.39; H, 4.06; N, 2.94; M, 11.88. Calcd. Mol.Wt. 459 (g/mole). IR ( $\nu$ ,  $cm^{-1}$ ): 3345br (OH), 1724sh (C=O

coumarin), 1615m (C=N), 1230 Sh (C-O), 936w and 858w ( $H_2O$  coordinated water), 534w (M-O), 446w (M-N). UV-Vis ( $\lambda$ , nm): 209 ( $\pi$ - $\pi^*$ ), 273( $\pi$ - $\pi^*$ ), and 336(n- $\pi^*$ ) transitions.  $\Lambda_m$  ( $\Omega^{-1} mol^{-1} cm^2$ ): 31.5.

##### [Fe(HL)Cl<sub>3</sub>].4H<sub>2</sub>O

Yield 85%; dark green solid, m.p >300 °C. Anal. Calcd. for  $Fe(C_{17}H_{13}NO_3Cl_3) \cdot 4H_2O$  (%): C, 38.24; H, 3.94; N, 2.62; M, 10.50. Found (%): C, 38.18; H, 3.90; N, 2.50, M, 10.42. Calcd. Mol.Wt. 533.5 (g/mole), IR ( $\nu$ ,  $cm^{-1}$ ): 3411br (OH), 1736sh (C=O coumarin), 1632sh (C=N), 1220sh (C-O), 936w and 870w ( $H_2O$  coordinated water), 541s (M-O), 482w (M-N). UV-Vis ( $\lambda$ , nm): 210 ( $\pi$ - $\pi^*$ ), 275 ( $\pi$ - $\pi^*$ ) and 331 (n- $\pi^*$ ) transitions.  $\Lambda_m$  ( $\Omega^{-1} mol^{-1} cm^2$ ): 41.5.

##### [Co(HL)Cl<sub>2</sub>.H<sub>2</sub>O].4H<sub>2</sub>O

Yield 75%; dark brown solid, m.p 290 °C. Anal. Calcd. for  $Co(C_{17}H_{13}NO_3Cl_2.H_2O) \cdot 4H_2O$  (%): C, 40.88; H, 4.61; N, 2.81; M, 11.82. Found (%): C, 40.79; H, 4.58; N, 2.76; M, 11.62. Calcd. Mol.Wt. 499 (g/mole). IR ( $\nu$ ,  $cm^{-1}$ ): 3369br (OH), 1736sh (C=O coumarin), 1621m (C=N), 1234sh (C-O), 930w and 858w ( $H_2O$  coordinated water), 565w (M-O), 431w (M-N). UV-Vis ( $\lambda$ , nm): 211 ( $\pi$ - $\pi^*$ ), 271 ( $\pi$ - $\pi^*$ ) and 328 (n- $\pi^*$ ) transitions.  $\Lambda_m$  ( $\Omega^{-1} mol^{-1} cm^2$ ): 31.4.

##### [Ni(HL)Cl<sub>2</sub>.H<sub>2</sub>O].2H<sub>2</sub>O

Yield 92%; dark green solid, m.p 280 °C. Anal. Calcd. for  $Ni(C_{17}H_{13}NO_3Cl_2.H_2O) \cdot 2H_2O$  (%): C, 44.06; H, 4.10; N, 3.02; M, 12.74, Found C, 43.97; H, 4.03; N, 2.98; M, 12.54. Calcd. Mol.Wt. 463 (g/mole). IR ( $\nu$ ,  $cm^{-1}$ ): 3440br (OH), 1736sh (C=O coumarin), 1615m (C=N), 1228sh (C-O), 930w and 858w ( $H_2O$  coordinated water), 501s (M-O), 428w (M-N). UV-Vis ( $\lambda$ , nm): 211 ( $\pi$ - $\pi^*$ ), 272 ( $\pi$ - $\pi^*$ ) and 334 (n- $\pi^*$ ) transitions.  $\Lambda_m$  ( $\Omega^{-1} mol^{-1} cm^2$ ): 42.6

##### [Cu(HL)Cl<sub>2</sub>.H<sub>2</sub>O].2H<sub>2</sub>O

Yield 87%; dark green solid, m.p 285 °C. Anal. Calcd. for  $Cu(C_{17}H_{13}NO_3Cl_2.H_2O) \cdot 2H_2O$  (%): C, 44.64; H, 4.06; N, 2.99; M, 13.58. Found (%): C, 43.57; H, 4.02; N, 2.87; M, 13.42. Calcd. Mol.Wt. 467.5 (g/mole). IR ( $\nu$ ,  $cm^{-1}$ ): 3345br (OH), 1724sh (C=O coumarin), 1621sh (C=N), 1220sh (C-O), 948w and 858w ( $H_2O$  coordinated water), 538s (M-O), 462w (M-N). UV-Vis ( $\lambda$ , nm): 207 ( $\pi$ - $\pi^*$ ), 281 ( $\pi$ - $\pi^*$ ) and 336 (n- $\pi^*$ ) transitions.  $\Lambda_m$  ( $\Omega^{-1} mol^{-1} cm^2$ ): 23.1.

##### [Zn(HL)Cl<sub>2</sub>.H<sub>2</sub>O].5H<sub>2</sub>O

Yield 88%; brown solid, m.p 290 °C. Anal. Calcd. for  $Zn(C_{17}H_{13}NO_3Cl_2.H_2O) \cdot 5H_2O$  (%): C, 39.01; H, 4.78; N, 2.68; M, 12.43 Found (%): C, 38.88; H, 4.74; N, 2.55; M, 12.40. Calcd. Mol.Wt. 523 (g/mole). IR ( $\nu$ ,  $cm^{-1}$ ): 3404br (OH), 1736sh (C=O coumarin), 1615m (C=N), 1228sh (C-O), 936w and 858w ( $H_2O$  coordinated water), 541s (M-O), 458w (M-N). UV-Vis ( $\lambda$ , nm): 205 ( $\pi$ - $\pi^*$ ), 271 ( $\pi$ - $\pi^*$ ) and 327 (n- $\pi^*$ ) transitions.  $\Lambda_m$  ( $\Omega^{-1} mol^{-1} cm^2$ ): 12.1.

##### [Cd(HL)Cl<sub>2</sub>.H<sub>2</sub>O].3H<sub>2</sub>O

Yield 89%; faint brown solid, m.p >300 °C. Anal. Calcd. for  $Cd(C_{17}H_{13}NO_3Cl_2.H_2O) \cdot 3H_2O$  (%): C,

38.20; H, 3.93; N, 2.62; M, 20.97. Found (%): C, 38.08; H, 3.91; N, 2.58; M, 21.13. Calcd. Mol. Wt. 534 (g/mole). IR ( $\nu$ ,  $\text{cm}^{-1}$ ): 3417br (OH), 1724sh (C=O coumarin), 1632sh (C=N), 1228sh (C-O), 948w and 858w ( $\text{H}_2\text{O}$  coordinated water), 538s (M-O), 462s (M-N).  $^1\text{H}$  NMR ( $\delta$  ppm): 6.1-6.9 (m, 9H, ArH), 1.72 (t, 3H,  $\text{CH}_3$ ), 11.68 (s, 1H, phenolic OH), UV-Vis ( $\lambda$ , nm): 210 ( $\pi$ - $\pi^*$ ), 273 ( $\pi$ - $\pi^*$ ) and 340 (n- $\pi^*$ ) transitions,  $\Lambda_m$  ( $\Omega^{-1} \text{mol}^{-1} \text{cm}^2$ ): 3.

## Results and Discussion

### 3.1. Elemental analysis and conductivity measurement

Elemental analysis is confirmed the suggested geometry with 1:1 Metal to ligand ratio, as shown in experimental part. Additionally, the molar conductivity ( $\Lambda_m$ ) is detected in DMF of 10<sup>-3</sup> M solutions for all complexes at room temperature. In brief, all complexes have a weak ionic nature (non-electrolytes), while conductivity fall in the range from 3.0 to 42.6  $\Omega^{-1} \text{mol}^{-1} \text{cm}^2$ . This indicated that the anions were involved in the coordination sphere [33].

### 3.2. FT-IR spectral study

The IR spectra exhibits that the bands associated with coordinated atoms in ligand were possess higher electron density whereas their bands after coordination are shifted towards lower frequencies. In instance, nitrogen atom in azomethine group exhibited reduction in electron density after coordination [34]. The band at 1655  $\text{cm}^{-1}$  belongs to azomethine  $\nu(\text{C}=\text{N})$  stretching vibration which showed slight decrease towards low frequencies in complexes in the range of 1615-1632  $\text{cm}^{-1}$ , moreover, may refer that configured bond was shorter than the original one [11, 13, 35, 36]. It also confirmed the coordination of azomethine N to the metal ions. Additionally, C=O stretching vibration which is assigned to the coumarin skeleton, found in the free Schiff base ligand at 1748  $\text{cm}^{-1}$ , showed a negative shift after coordination (1714-1736  $\text{cm}^{-1}$ ) which support its involvement in coordination to metal ions [36]. Further, the IR spectrum of Schiff base ligand showed broad band at 3447  $\text{cm}^{-1}$  assigned to O-H stretching vibration [35]. This band exhibits negative shift to 3345-3417  $\text{cm}^{-1}$  that reflects further confirmation of its association in coordination [35]. The coordination of phenolic OH in coordination is further confirmed by the shift of  $\nu(\text{C}-\text{O})$  stretching vibration from 1235  $\text{cm}^{-1}$  in the free ligand to 1220-1234  $\text{cm}^{-1}$  in the IR spectra of the complexes [37]. Furthermore, the bands in the range of 428-486  $\text{cm}^{-1}$  assigned to the stretching vibration mode of  $\nu(\text{M}-\text{N})$  [37-39], while the bands at 501-565  $\text{cm}^{-1}$  indicates  $\nu(\text{M}-\text{O})$  stretching mode [38, 40, 41]. Likewise, the existence of coordinated water molecules in complexes was confirmed by two weak bands in the regions of 918-948 and 858-870  $\text{cm}^{-1}$  due to  $\nu(\text{H}_2\text{O})$  rocking and wagging modes of vibrations, respectively. The IR results revealed that the Schiff

base ligand behaved as a neutral tridentate ligand coordinated to the metal ions through azomethine nitrogen and phenolic oxygen in addition to carbonyl oxygen atoms.

### 3.3. $^1\text{H}$ NMR spectral studies of HL and its complexes

$^1\text{H}$  NMR spectrum of Schiff base ligand displays proton NMR signals for aromatic,  $\text{CH}_3$  and phenolic OH protons at 6.4-7.3 ppm (m, 9H, ArH), 1.81 (t, 3H,  $\text{CH}_3$ ) and 11.5 ppm (s, 1H, Phenolic OH), respectively [32]. Moreover,  $^1\text{H}$  NMR spectrum of Cd(II) complex revealed that the O-H proton exhibits a significant chemical shift, recorded at 11.68 ppm that further confirmed the coordination of phenolic oxygen to the metals ion during formation of metal complex without proton displacement.

### 3.4. Mass spectral studies

MS is a crucial tool in interpreting the stoichiometric composition of ligands and complexes. The mass spectrum of the Ligand is in well matching with its calculated Molecular mass that  $m/z = 281$  amu (calcd = 279.29 amu), while The mass spectrum of the dehydrated Cu(II) complex displays a molecular ion peak at  $m/z = 432$  amu (calcd = 431.757 amu). The detected peaks are in good matching with the proposed formula as designated by the microanalytical data shown in Figure 1.

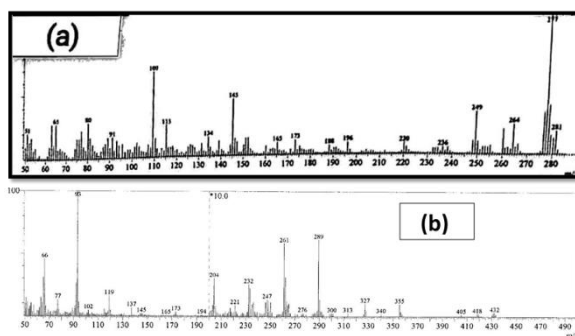


**Figure (1).** The mass spectra of (a) Schiff base ligand (HL) and (b) Cu(II) complex.

### 3.5. Surface morphology

Figure 2 exhibits SEM micrographs of some selected Nano-complexes that Cobalt complex records 20 nm as average grain size, while Ni-complex shows about 17.5 nm, however cadmium displays the smallest which records average grain size 14.8 nm. Additionally, Co(II) complex shows highest biological activity due to its rough surface as shown in Fig. 2a. That surface roughness is directly proportional to biological activity [42-44].

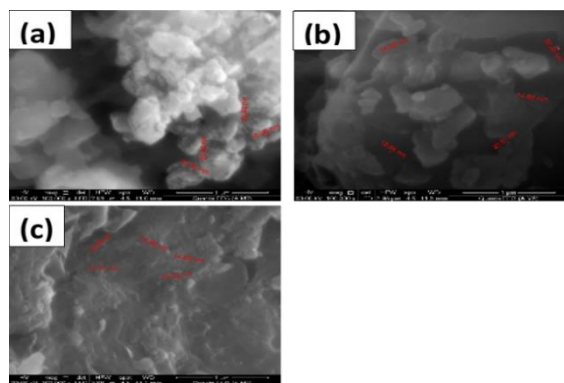


Figure (2). FE-SEM micrographs of (a) Co(II), (b) Ni(II) and (c) Cd(II) metal complexes.

### 3.6. Thermal analysis studies (TG and DTG)

The TGA curve for ligand is shown in Table (1). Ligand showed two decomposition steps. The first step occurred in the temperature range 92-270 °C and corresponding to loss of 66.23% with a practical weight loss of (calc. 66.41%). The second step in the temperature range 270- 800 °C corresponding to loss of 32.64% with a practical weight loss of (calc. 32.58%). the total weight loss amounted to 98.87% (Calcd 98.99%).

Thermogravimetric (TG) curve for [Cr(HL)Cl<sub>3</sub>].3H<sub>2</sub>O complex showed four weight loss steps. The first, second and third decomposition events occurred within the temperature range of 25-360 °C, with three temperature peaks at 40, 129, and 286 °C and correspond to the loss of three water molecules, methane and hydrochloride molecules. The last step can be assigned to the loss of chlorine and C<sub>16</sub>H<sub>6</sub>NO<sub>1.5</sub> fragments within the temperature range 360-830 °C with overall estimated mass loss of 81.20% (calculated mass loss = 81.71%) leaving metal oxide ½Cr<sub>2</sub>O<sub>3</sub> residue.

[Mn(HL)Cl<sub>2</sub>(H<sub>2</sub>O)].2H<sub>2</sub>O complex gave decomposition pattern of multi-steps with six maximum at 60, 87, 121, 156, 196 and 285 °C which representing the loss of C<sub>9</sub>H<sub>9</sub>O<sub>4</sub> fragment, CH<sub>8</sub>NO fragment and two hydrochloride molecules within the temperature range from 30 to 900 °C with an estimated weight loss of 64.83% (calculated mass loss = 66.2%). MnO contaminated with carbon was the residue of decomposition.

The [Cd(HL)Cl<sub>2</sub>.H<sub>2</sub>O].3H<sub>2</sub>O chelate showed four decomposition steps. The first two steps exhibited in the temperature range from 30 to 270 °C with two maxima at 197 and 230 °C. These steps may reflect loss of 3H<sub>2</sub>O and loss of CH<sub>4</sub> and H<sub>2</sub>O. The third step showed peak at 320 °C in the temperature range of 270-355 °C which may due to weight loss of 25.26% (calculated weight loss = 27.1%). This step corresponds to elimination of C<sub>9</sub>H<sub>5</sub>O<sub>2</sub> fragment. The

final step showed peak at 596 °C in the temperature range of 355-650 °C which was due to weight loss of 30.77% (calculated weight loss = 30.30%) and leaving CdO contaminated with carbon as the residue of decomposition. The overall weight loss amounted to 82.92% (calcd. = 83.67%).

The [Fe(HL)Cl<sub>3</sub>].4H<sub>2</sub>O complex decomposed from temperature 30 to 900 °C with three steps as explained. The peaks with maximum temperatures at 45.79, 169.62 and 543.96 °C and elimination of water of hydration then of coordination with hydrochloride molecule and water molecule and in the end C<sub>15</sub>H<sub>12</sub>NO<sub>1.5</sub>Cl fragment with an estimated weight loss of 76.98% (calcd. = 76.4%) were assigned. At the end of the thermogram, the metal oxide ½Fe<sub>2</sub>O<sub>3</sub> contaminated with carbon was the residue of decomposition.

The [Co(HL)Cl<sub>2</sub>(H<sub>2</sub>O)].4H<sub>2</sub>O chelate was thermally decomposed in three steps within the temperature range from 30 to 900 °C. The first decomposition step with an estimated mass loss of 14.51% (calcd. = 14.11%) was occurred within the temperature range from 30 to 100 °C with temperature maximum at 60 °C. This step may be attributed to the liberation of the four hydrated water molecules. The second decomposition step within the temperature range of 100-170 °C with maximum temperature at 133 °C, can accounted to the loss of hydrochloride molecule with estimated mass loss of 8.57% (calcd. = 7.21%). The third decomposition step in the temperature range of 170-900 °C with maximum temperature at 678 °C correspond to the loss of C<sub>13</sub>H<sub>12</sub>Cl<sub>2</sub>NO<sub>3</sub> fragment with estimated mass loss of 61.00% (calculated mass loss = 60.90%). At the end of the curve, the metal oxide CoO contaminated with carbon was the final product with total estimated mass loss of 84.10% (calcd. = 84.75%). Thermogravimetric curve for [Ni(HL)(Cl<sub>2</sub>)(H<sub>2</sub>O)].2H<sub>2</sub>O complex showed three weight loss events.

The first step of decomposition occurred within the temperature range of 30-105 °C, with a maximum temperature at 47 °C and correspond to the loss of two water molecules of hydration with estimated mass loss of 6.30% (calculated mass loss = 8.40%). The second and third steps of decomposition occurred in the range of 105-870 °C with two maxima at 129 and 514 °C. The second step correspond to the loss of chlorine molecule but the final step is corresponding to loss of C<sub>10</sub>H<sub>13</sub>NO<sub>2</sub> fragment leaving metal oxide NiO contaminated with carbon atoms as residue. The overall weight loss amounted to 63.42% (calculated mass loss = 66.10%).

**Table 1.** Thermal analysis results (TG and DTG) of HL and its metal complexes.

Complex	TG range (°C)	DTG <sub>max</sub> (°C)	n*	Mass loss Estim (Calcd) %	Total mass loss %	Assignment	Residues
HL	92-270 270-800	185 375	1 1	66.23(66.41%) 32.64(32.58%)	98.87 (98.99)	- Loss of C <sub>11</sub> H <sub>8</sub> NO <sub>2</sub> -Loss of C <sub>6</sub> H <sub>5</sub> O	----- -
[Co(HL)Cl <sub>2</sub> .H <sub>2</sub> O].4H <sub>2</sub> O	30-100 100-170 170-900	60 133 678	1 1 1	14.51 (14.44) 8.570 (7.21) 61.00 (60.90)	84.10 (84.75)	- Loss of 4H <sub>2</sub> O - Loss of HCl Loss of C <sub>13</sub> H <sub>12</sub> Cl <sub>2</sub> NO <sub>3</sub> .	4C + CoO
[Cr(HL)Cl <sub>3</sub> ].3H <sub>2</sub> O	25-109 109-200 200-360 360-830	40 129 286 446	1 1 1 1	10.88 (9.98) 9.337 (10.50) 13.54 (14.20) 47.47 (47.03)	81.20 (81.71)	-- Loss of 3H <sub>2</sub> O - Loss of HCl, CH <sub>4</sub> - Loss of Cl <sub>2</sub> - Loss of C <sub>10</sub> H <sub>6</sub> NO <sub>1.5</sub> .	1/2Cr <sub>2</sub> O <sub>3</sub>
[Cu(HL)Cl <sub>2</sub> .H <sub>2</sub> O].2H <sub>2</sub> O	59-105 105-350 350-900	76 166 526	1 1 1	7.10 (7.70) 23.92 (22.60) 37.87 (37.10)	67.35 (68.80)	- Loss of 2H <sub>2</sub> O. - Loss of H <sub>2</sub> O, 2HCl, CH <sub>4</sub> . - Loss of C <sub>10</sub> H <sub>8</sub> NO <sub>2</sub> .	6C + CuO
[Cd(HL)Cl <sub>2</sub> .H <sub>2</sub> O].3H <sub>2</sub> O	192-216 216-270 270-355 355-650	197 230 320 596	1 1 1 1	11.64 (10.19) 6.127 (6.36) 25.26 (27.10) 30.77 (30.30)	82.92 (83.67)	- Loss of 3H <sub>2</sub> O - Loss of CH <sub>4</sub> , H <sub>2</sub> O -- Loss of C <sub>9</sub> H <sub>5</sub> O <sub>2</sub> . - Loss of Cl <sub>2</sub> , C <sub>6</sub> H <sub>4</sub> N	CdO+C
[Fe(HL)Cl <sub>3</sub> ].4H <sub>2</sub> O	30- 103 103-450 450-890	45.79 169.62 543.96	1 1 1	13.81 (14.1) 12.05 (10.5) 51.13 (51.80)	76.98 (76.40)	- Loss of 4H <sub>2</sub> O - Loss of HCl, H <sub>2</sub> O - Loss of C <sub>15</sub> H <sub>12</sub> NO <sub>1.5</sub> Cl	2C + ½ Fe <sub>2</sub> O <sub>3</sub>
[Mn(HL)Cl <sub>2</sub> .H <sub>2</sub> O].2H <sub>2</sub> O	30- 350 350- 900	60,87,121,156, 196, 285 621	6 1	39.53(39.40) 25.34 (26.80)	64.83 (66.20)	- Loss of C <sub>9</sub> H <sub>9</sub> O <sub>4</sub> . - Loss of CH <sub>8</sub> NO <sub>2</sub> HCl	7C + MnO
[Ni(HL)Cl <sub>2</sub> .H <sub>2</sub> O].2H <sub>2</sub> O	30 -105 105- 202 202- 870	47 129 514	1 1 1	6.34 (8.40) 14.76 (15.10) 42.36 (42.60)	63.42 (66.10)	- Loss of 2H <sub>2</sub> O - Loss of Cl <sub>2</sub> . - Loss of C <sub>10</sub> H <sub>13</sub> NO <sub>2</sub>	7C + NiO
[Zn(HL) Cl <sub>2</sub> .H <sub>2</sub> O ].5H <sub>2</sub> O	30- 215 215- 250 250-800	58.08 237.68 502.36	1 1 1	18.60 (17.20) 19.64 (19.81) 30.65 (33.45)	68.85 (70.45)	- Loss of 5H <sub>2</sub> O - Loss of Cl <sub>2</sub> , CH <sub>3</sub> H <sub>2</sub> O. - Loss of CH <sub>9</sub> NO <sub>2</sub>	6C + ZnO

\* n = number of decomposition steps

On the other hand, [Cu(HL)(Cl<sub>2</sub>)(H<sub>2</sub>O)].2H<sub>2</sub>O complex was thermally decomposed in three steps within the temperature range from 30 to 900 °C. The first and next two decomposition steps were with an estimated mass loss of 67.35% (calcd. = 68.80%) occurred with three maxima at 76, 166 and 526 °C. These steps may be attributed to the loss of the hydrated water, methane molecule, coordinated water, two hydrochloride molecules and C<sub>10</sub>H<sub>8</sub>NO<sub>2</sub> molecules. CuO contaminated with carbon atoms was remained as residue.

The TG curve of [Zn(HL)(Cl<sub>2</sub>)(H<sub>2</sub>O)].5H<sub>2</sub>O complex showed peak at 58 °C in the temperature range of 30-215 °C which was due to loss of 5H<sub>2</sub>O with mass loss of 18.60% (calculated weight loss = 17.20%). This step may assign to the loss of five water molecules and the second step assigned to the loss of methane molecule, coordinated water and hydrochloride molecule at the temperature peak of 237 °C. The final step of the thermal decomposition, which occurred in the range of 250-800 °C with maximum at 502 °C, may assigned to the loss of CH<sub>9</sub>NO<sub>2</sub> molecule (mass loss = 30.65%; calcd. = 33.45%). At the end of the curve, the metal oxide ZnO contaminated with carbon atoms was the residue with total weight loss amounted to 68.85% (calcd. = 70.45%).

### 3.7. Electronic spectral studies

The absorption spectra of the complexes are measured in ethanol as well as Schiff base ligand. Coordination is confirmed by absorption band intensity that ligand exhibited higher bands intensities than complexes. Moreover, ligand spectrum displayed bands at 216, 274, and 334 nm corresponding to  $\pi$ - $\pi^*$ ,  $\pi$ - $\pi^*$ , and  $n$ - $\pi^*$  transitions, respectively. These transitions can be assigned to the presence of azomethine and other chromophores within the Schiff base ligand [45]. On the other hand, complexes displayed bands in range from 208 to 212, 272 to 274 and 330 to 334 nm which almost showed hypochromic shift due to coordination [32].

### 3.8. Geometry optimization

#### 3.8.1. Optimized Molecular structures of Schiff base

Schiff base molecular structure has been optimized by HF and DFT levels of calculations through 3-21G basis set (Figure 3). Geometrical optimization has been run for obtaining the lowest energy configuration from the initial guess of the geometry. Additionally, the wave functions are calculated till detecting the most stable molecule and forces values become zero. Moreover, geometrical optimization detects minima on a potential energy surface (PES). Furthermore, convergence criteria

Table 2. Some selected bond parameters of HL ligand			
Bond	Bond lengths (Å) (HF)	Angle	Bond angles (°)(HF)
C1-C2	1.394	C1-C2-C3	120.041
C2-C3	1.376	C2-C3-C4	119.867
C3-C4	1.394	C3-C4-C5	120.71
C4-C5	1.379	C4-C5-C6	118.794
C5-C6	1.381	C5-C6-C1	121.5
C6-C1	1.383	C6-C1-C2	119.07
C1-C11	1.447	H7-C2-C3	120.589
C11-C13	1.334	H7-C2-C1	119.37
C12-C13	1.4645	H8-C3-C2	120.155
C12-O15	1.373	H8-C3-C4	119.978
C12-O16	1.203	H9-C4-C3	119.82
C2-H7	1.072	H9-C4-C5	119.48
C3-H8	1.070	H10-C5-C4	121.876
C4-H9	1.071	H10-C5-C6	119.33
C5-H10	1.069	C1-C6-O15	119.78
C13-C14	1.497	C6-O15-C12	124.65
C11-H34	1.07	O15-C12-C13	115.65
C14-C17	1.512	C12-C13-C11	120.39
C17-H18	1.08	C13-C11-C1	121.99
C17-H19	1.08	C11-C1-C6	117.5
C17-H20	1.08	O15-C12-O16	118.07
C14-N21	1.26	O16-C12-C13	126.27
N21-C24	1.42	C13-C11-H34	120.323
C23-C24	1.39	H34-C11-C1	117.68
C24-C25	1.383	C11-C13-C14	122.76
C25-H30	1.07	C14-C13-C12	116.82
C26-O32	1.375	C14-C17-H18	109.52
O32-H33	0.966	C14-C17-H19	110.722
C26-C27	1.38	C14-C17-H20	109.785
C27-H31	1.07	C17-H14-N21	119.51
C22-C27	1.39	C14-N21-C24	126.23
C22-H28	1.07	C25-C24-N21	122.36
C22-C23	1.38	C23-C24-N21	117.75
C23-H29	1.07	C23-C24-C25	119.74
		C24-C23-H29	119.15
		H29-C23-C22	121.26
		C23-C22-H28	119.74
		C27-C22-H28	119.38
		C23-C22-C27	120.88
		C22-C27-H31	120.26
		H31-C27-C26	120.39
		C22-C27-C26	119.34
		C25-C26-C27	120.255

involved the forces at a certain point and the shift of the next step estimate whether a stationary point has been found to find out whether the geometry optimization is a minimum. Intermolecular interactions have been computed using HF and DFT levels of calculations, as mentioned in Table 2. DFT involved electron correlation effect on the intermolecular stabilization energy, thus it gives more accurate results [46]. Optimized arrangement of atoms in ligand showed almost similar results in HF and DFT.

Frontier orbitals included highest occupied molecular orbital (HOMO) and lowest unoccupied molecular orbital (LUMO), where the gap between them is an indicator of reactivity and kinetic stability of the molecule. HOMO and LUMO orbitals topologically have almost pure  $\pi$ -character orbitals in both HF and DFT results. MEP exhibited the electronic distribution upon the surface of computed molecule, the size,

sites [47, 48]. According to colour grading style, three donating atoms upon the ligand surface displayed electron-rich sites which has red colour (favour site for Metallic shape, besides electrostatic potential in color grading style, thus able to predict active electrophilic attack), thus the compound is tridentate ligand (Figure 4). However, the electron-poor sites has blue color (favor site for donor atoms nucleophilic attack) [49].

Furthermore, reactivity parameters such as total energy and HOMO and LUMO energies are calculated in addition to selected quantum chemical parameters of Schiff base ligand (HL) are tabulated in Table (3), as  $\Delta E$ , absolute electronegativities,  $\chi$ , chemical potentials,  $\mu$ , absolute hardness,  $\eta$ , absolute softness,  $\sigma$ , global electrophilicity,  $\omega$ , global softness,  $S$ , and additional electronic charge,  $\Delta N_{\max}$ , were calculated according to the following equations:

$$\Delta E = E_{LUMO} - E_{HOMO} \quad (1)$$

$$\chi = \frac{-(E_{HOMO} + E_{LUMO})}{2} \quad (2)$$

$$\eta = \frac{E_{LUMO} - E_{HOMO}}{2} \quad (3)$$

$$\sigma = \frac{1}{\eta} \quad (4)$$

$$Pi = -\chi \quad (5)$$

$$S = \frac{1}{2\eta} \quad (6)$$

$$\omega = \frac{Pi^2}{2\eta} \quad (7)$$

$$\Delta N_{\max} = -\frac{P_i}{\eta} \quad (8)$$

Electrophilicity index ( $\omega$ ) determines toxicity and the reactivity of various active sites.  $\eta$  and  $\sigma$  indexes, represent the molecular stability and reactivity. The softness indexes and global hardness are the vice versa image for each other [49, 50]. The positive, high electrophilicity index ( $\chi$ ) value reflected the biological reactivity of ligand and stability, besides the electronic chemical potential must be negative [51].

Computed molecular units are studied in terms of geometry, different parameters and charges. Ligand structure has sigma skeleton,  $\pi$  conjugation core and electronegative atoms. Mulliken atomic

charge calculation has a vital role in quantum chemical calculation to molecular system that individual atomic charges influence dipole moment, polarizability, electronic structure directly [52]. Comparing charge values of each atom of ligand (Figure 5), difference between DFT and HF level of calculation values has been explained by electron correlation [46]. Donating atoms in coordination compounds are estimated through electronic charge on it. Mulliken population analysis has computed with same geometry optimization root. HF and DFT results show slightly difference that all hydrogen have positive charge, nitrogen atom carries negative charge, oxygen atoms show negative charge. Mulliken population analysis and MEP results are matching.

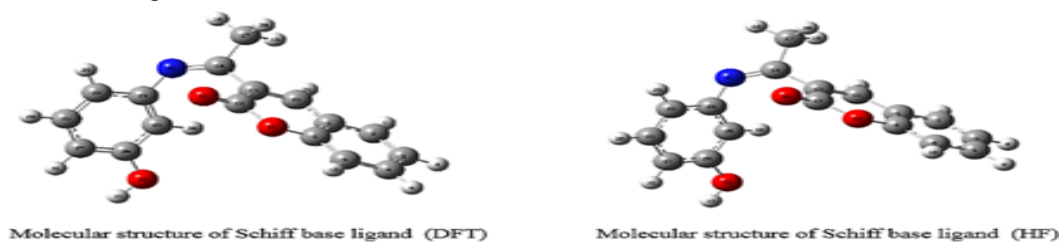


**Figure (3).** Optimized geometry of Schiff base molecular structure by HF and DFT levels of calculations through 3-21G basis set.

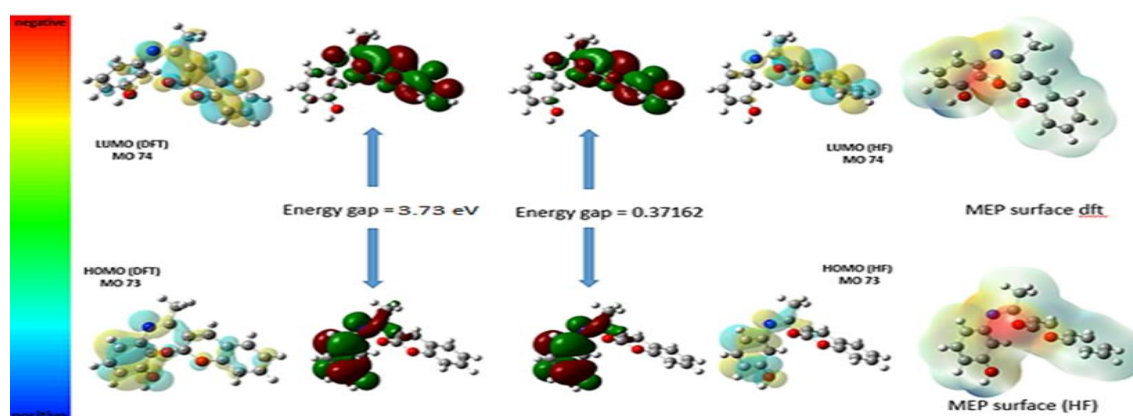


**Figure (4).** Frontier Molecular orbitals with MEP of HL by HF and DFT levels of calculations

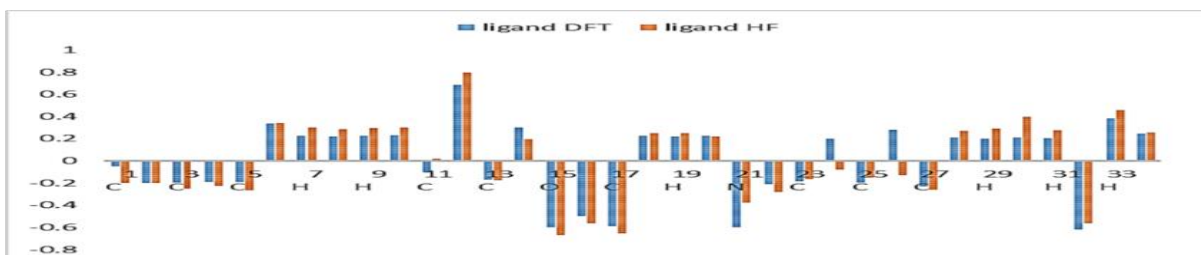


**Figure (5).** Total atomic charges on atoms of ligand, from HF and DFT Mulliken population analysis

Table 3. Selected quantum chemical parameters of Schiff base ligand (HL) using HF and DFT functions

	$E_{\text{HOMO}}$	$E_{\text{LUMO}}$	$\Delta E$	$X$	$n$	$\sigma$	$Pi$	$S$	$\omega$	$\Delta N_{\text{max}}$
<b>HF</b>	-8.615	1.497	10.11	3.559	5.056	0.198	-3.559	2.528	1.253	0.704
<b>DFT</b>	-5.93	-2.194	3.734	4.062	1.868	0.535	-4.062	0.934	4.416	2.175

Table 4. Selected quantum chemical parameters of Schiff base ligand (HL) and its Cu(II) complex (LANDZ2).

<b>Bond lengths (Å)</b>	<b>HL</b>	<b>[Cu(HL)Cl<sub>2</sub>.H<sub>2</sub>O].2H<sub>2</sub>O</b>
C(14)-N(21)	1.26	1.29
N(21)-C(24),	1.41	1.42
O(32)-H(33)	0.96	0.97
Cu(37)-O(38)	-----	2.16
Cu(37)-N(21)	-----	3.58
Cu(37)-Cl(35)	-----	2.28
<b>Bond angles (°)</b>		
O(38)- Cu(37)-N(21)	-----	102.8
O(32)- Cu(37)-O(38)	-----	106.6
N(21)- Cu(37)-Cl(35)	-----	114.6
N(21)- Cu(37)-Cl(36)	-----	77.23034
O(32)-Cu(37)-Cl(36)	-----	73.38261
<b>The calculated quantum chemical parameters</b>		
<b>E (a.u.)</b>	-930.9088	-1352.97
Dipole moment (Debye)	6.3655	11.18
$E_{\text{HOMO}}$ (eV)	-5.93	-6.57
$E_{\text{LUMO}}$ (eV)	-2.194	-2.95
$\Delta E$ (eV)	3.734	3.62
$\chi$ (eV)	4.062	4.76
$\eta$ (eV)	1.868	1.81
$\sigma$ (eV) <sup>-1</sup>	0.535	0.55
$Pi$ (eV)	-4.062	-4.76
$S$ (eV) <sup>-1</sup>	0.934	0.28
$\omega$ (eV)	4.416	6.253
$\Delta N_{\text{max}}$	2.175	8.62

### 3.8.2. Optimized molecular structure of Cu(II) complex

Copper(II) complex have been performed at DFT/LANL2DZ level (Figure 6). Comparing between ligand and complex parameters refer to intermolecular interactions such as bond length and angles, total atomic charge and dipole moments. Elongation of some selected bonds confirmed coordination occurrence that bond length of azomethine group (C=N) is changed from 1.26 to 1.29 Å, phenolic (O-H) changed from 0.96 to 0.97 Å while it was 1.41 in ligand and changed to 1.42 Å in case of [Cu(HL)Cl<sub>2</sub>(H<sub>2</sub>O)] complex (Table 6). The smaller molecular orbital gap

is the more polarizable and the higher chemical reactivity, low kinetic stability and is also classified as as soft molecule [53]. The frontier orbital gaps of ligand / Cu(II) complex are to be 3.73/3.62 eV which clearly shows that copper complex is more reactive and polarizable than ligand according to DFT calculation. HOMO and LUMO orbitals topologically have almost pure  $\pi$ -character orbitals in both HF and DFT results (Figure 7) but in case of complex their shape is changed and acquired hybrid characters and this due to the influence of donor-acceptor interaction in complex case [54].

The LUMO in Cu-complex is distributed over copper metal besides coordinated chlorine atoms, while HOMO is distributed over copper metal besides coordinated chlorine atoms, while HOMO is distributed over entire complex except benzene attached in pyrone ring. Based on color grading style in MEP, homogeneous distribution of charge density, however, showed a greater negative charge on their surface, thus MEP results matching with Mulliken population analysis.

A detailed description is done by a comparative analysis of the atomic charges in ligand and complex. Negative shift of electron density on some selected atoms confirmed donation characteristics as listed in Table (5).

**Table 5.** Total atomic charges on selected atoms in ligand and complex, from DFT Mulliken population analysis

Donation atoms	DFT		
	Ligand	Cu-HL	$\Delta Q$
N21	-0.6	-0.098	-0.5
O32	-0.6	-0.48	-0.14
O16	-0.5	-0.3	-0.2

On the other hand, the mentioned quantum chemical parameters in Table (4) pointed out that Cu(II) complex has excellent biological activity based on

high  $\omega$  value. Moreover, the energies of the HOMO and LUMO in the complex were negative values, which showed the stability of isolated complex, in addition to showing higher negativity in complex that reflects strong coordination bonds. Furthermore, the total energy of Cu(II) complex was higher than free ligand, which indicated greatly the stability of the isolated solid complex (Figure 8). Besides, the small energy gap can be associated with a high chemical reactivity, low kinetic stability and reflects to efficient electronic charge transfer interaction making the molecule highly polarizable, while the HOMO level localized on the entire complex except benzene ring attached to pyrone ring, which indicated the preferable sites for nucleophilic attack to the central metal atom [55]. The positive electrophilicity index ( $\chi$ ) value reflected the acceptance of electrons ability of ligand molecule from the surrounding that stability increase, and energy decreased by accepting electronic charge. so, the electronic chemical potential must be negative [56]. Additionally, the Cu(II) complex showed higher values of dipole moments than the free ligand. Finally, the smaller energy gap, the higher chemical reactivity, low kinetic stability and reflects clear electronegativity difference and electron transfer interaction so the molecule highly polarizable.

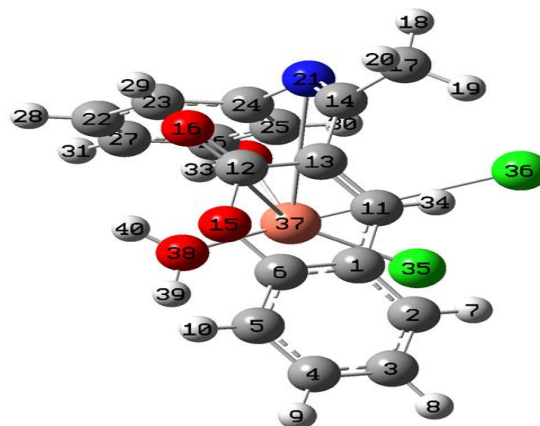


**Figure (6).** Optimized molecular structure of octahedral Cu(II) complex.

### 3.9. Biological activity

Antibacterial activity was tested in vitro against *Streptococcus aureus* and *Escherichia coli*. Additionally, fungicidal activity was screened in vitro against *Aspergillus flavus* and *Candida albicans* (see Figure 9). Moreover, chelation effect displays antibacterial effectiveness that Complexes belong polar and nonpolar portions, representing hydrophilic and lipophilic nature promoted cell membrane permeation into cells and tissues (liposoluble). Further, It is well known that metal complexes have higher antibacterial activity than the associated free Schiff base ligand which can be attributed to the

chelation of the Schiff base with metal ions as metal chelates displaying both polar and non-polar properties [13]. This makes them suitable for penetration into cells and tissues. The polarity of the metal ion will be decreased to a greater extent because of the overlap of the ligand orbital upon complexation, and partial sharing of the positive charge of the metal ion with donor groups.

Chelation enhances the delocalization of  $\pi$ -electrons over the whole chelating ring and induces the penetration of complexes into lipid membranes. It also increases the lipophilic and hydrophilic nature of the central metal ions contributing to liposolubility and permeability through the lipid layer of cell membranes. Furthermore, lipophilicity, which is responsible for the rate of entry of molecules into cells, is improved by coordination, so a metal complex can become more active than the free Schiff base ligand [13]. Additionally, ligand shows lower anti-bacterial and fungal activity that chelation enhance  $\pi$ -electrons delocalization over chelate ring and the penetration of the complexes into lipid membranes [57].

The complexes haven't any activities against *Aspergillus flavus*. Furthermore,

[Co(HL)Cl<sub>2</sub>.H<sub>2</sub>O].4H<sub>2</sub>O complex is the only compound displays activity against *Candida albicans* (Table 6). In addition to recording the highest activity against *Streptococcus aureus* with inhibition area 17 mm, while against *Escherichia coli* it records 14 mm, and 12 mm against *Candida albicans*. Thus, Co(II) complex shows highest biological activity due to its rough surface as shown in Fig. 2a as mentioned in surface morphology section where the surface roughness is directly proportional to biological activity [42-44].

### 3.10. Anticancer activity

It is obvious that Co(II), Ni(II) and Mn(II) complexes exhibit excellent effectiveness against breast cancer cells with small quantities (Table 7). Additionally, IC<sub>50</sub> (the concentration of the compound in  $\mu\text{g}/\text{mL}$  that inhibits proliferation of the cells by 50% as compared to the untreated control cells) values of the investigated compounds have been recorded 30.4, 23.1, and 22.2  $\mu\text{g}/\text{mL}$  for Co(II), Ni(II) and Mn(II) complexes, respectively (Figure 10).

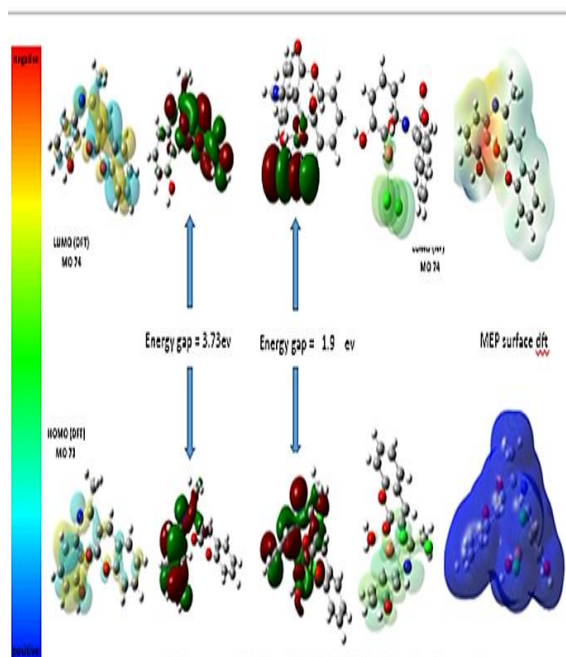


**Figure (7).** The Molecular orbital compositions, MEP and band gap of the frontier molecular orbital for HL ligand in DFT and its Cu(II) complex.

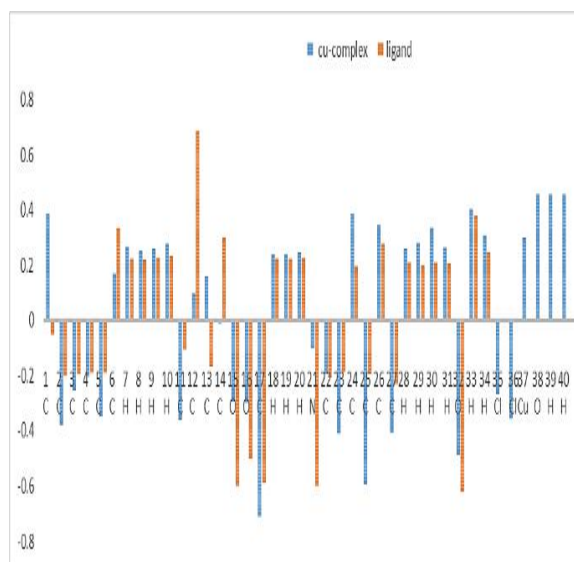


**Figure (8).** Total atomic charges on atoms in HL ligand and Cu(II) complex, DFT Mulliken population analysis

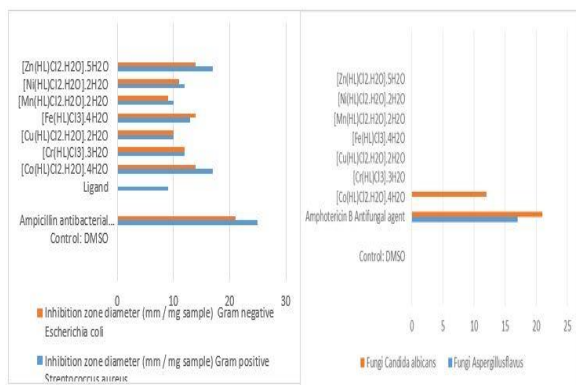


**Figure (9).** Anti-bacterial and anti-fungal activity of HL ligand and its metal complexes.

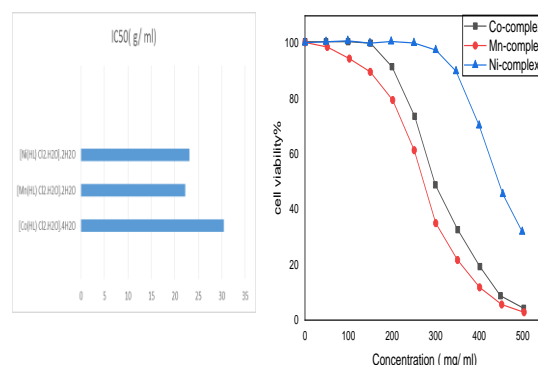


**Figure (10).** Cell viability and  $IC_{50}$  of metal complexes

**Table 6.** *In vitro* antibacterial and antifungal activity of Schiff base ligand and its metal

	Inhibition zone diameter (mm / mg sample)			
	Gram positive	Gram negative	Fungi	
	<i>Streptococcus aureus</i>	<i>Escherichia coli</i>	<i>Aspergillus flavus</i>	<i>Candida albicans</i>
Control: DMSO	0	0	0	0
Ampicillin (Antibacterial agent)	25	21	--	--
Amphotericin B (Antifungal agent)	--	--	17	21
HL	9	9	0	0
$[Co(HL)Cl_2H_2O] \cdot 4H_2O$	17	14	0	12
$[Cr(HL)Cl_2] \cdot 3H_2O$	12	12	0	0
$[Cu(HL)Cl_2H_2O] \cdot 2H_2O$	10	10	0	0
$[Fe(HL)Cl_2] \cdot 4H_2O$	13	14	0	0
$[Mn(HL)Cl_2H_2O] \cdot 2H_2O$	10	9	0	0
$[Ni(HL)Cl_2H_2O] \cdot 2H_2O$	12	11	0	0
$[Zn(HL)Cl_2H_2O] \cdot 5H_2O$	17	14	0	0

**Table 7.** The effect of different concentrations of tested compounds on human breast cancer cell line MCF-7.

Complex	Concn. ( $\mu\text{g/ml}$ )	Cell viability% (MCF7)					$IC_{50}$ ( $\mu\text{g/ml}$ )
		0.0	62.5	125	250	500	
$[Co(HL)Cl_2H_2O] \cdot 4H_2O$	100	32.91	19.74	8.53	4.17	30.4	
$[Mn(HL)Cl_2H_2O] \cdot 4H_2O$	100	20.48	11.62	6.08	2.84	22.2	
$[Ni(HL)Cl_2H_2O] \cdot 4H_2O$	100	89.52	70.34	46.28	31.49	23.1	

### 3.11. Molecular modeling: Docking Study

Molecular docking exhibits an optimized conformation for both the protein and prepared compounds with relative orientation between them such that the free energy of the overall system was minimized. Moreover, in this study, computation is involved Schiff base ligand (HL) and breast cancer mutant 4xo7. The results showed a good arrangement between Schiff base ligand (HL) and 4xo7 receptor as shown in Figure 11. The theoretically computed energy was reported in Table 8.

**Table 8.** Energy values obtained in docking calculations of Schiff base ligand (HL) with receptors of breast cancer mutant.

Ligand	Receptor	interaction	distance	E (kcal/mol)
6-ring	N LYS 270 (A)	$\pi$ -H	3.92	-0.7
6-ring	6-ring TYR 216 (A)	$\pi$ - $\pi$	3.63	0

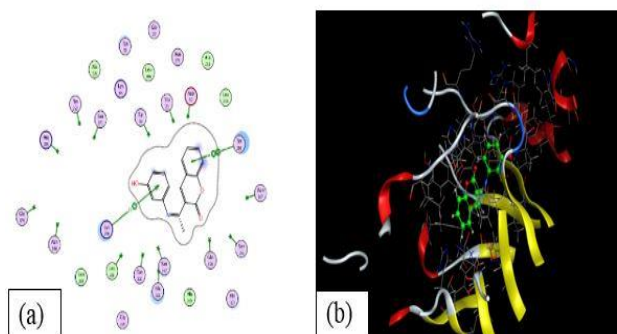


**Figure (11).** (a) 2D plot of interaction between Schiff base ligand (HL) and receptor of breast cancer mutant (4xo7) and (b) 3D plot.

#### 4. Conclusion

The novel Schiff base ligand with coumarin nucleus has been synthesized via the condensation of 3-acetyl coumarin with 3-aminophenol. Ligand and copper complex molecular optimization, besides molecular docking between Schiff base ligand (HL) and the receptors of breast cancer were executed. The novel prepared complexes were characterized by elemental analysis, molar conductivity, spectroscopic techniques (IR, <sup>1</sup>H NMR, mass spectrometry, UV–Vis), and thermal (TG/DTG) to predict their structures. The complexes exhibited octahedral complexes with 1:1 metal to ligand ratio. Additionally, antibacterial activity has been screened against *Streptococcus aureus* and *Escherichia coli*. Additionally, fungicidal activity was done in vitro against *Aspergillus flavus* and *Candida albicans*, using the disc diffusion method. The [Co(HL)Cl<sub>2</sub>.H<sub>2</sub>O].4H<sub>2</sub>O complex exhibited the maximum antimicrobial effect of the examined complexes, besides is the only compound that showed activity against *Candida albicans*. The [Mn(L)Cl<sub>2</sub>.H<sub>2</sub>O].4H<sub>2</sub>O complex was assessed in human cancer (MCF-7 cells viability) which showed lowest IC<sub>50</sub>.

#### Funding sources

Research does not fund.

#### Acknowledgment

It is a great pleasure to acknowledge my deepest thanks to Chemistry Department, Faculty of Science, Cairo University, for supporting and comprehensive advice to my work.

#### References

- [1] Shen Y, Zhang X, Liang L, Yue J, Huang D, Xu W, et al. Mitochondria-targeting supra-carbon dots: Enhanced photothermal therapy selective to cancer cells and their hyperthermia molecular actions. *Carbon* 2020;156:558-67.
- [2] Geneva. antimicrobial-resistance World Health Organization, Antimicrobial Resistance Fact Sheet 2018.
- [3] L.B. Rice. Federal funding for the study of antimicrobial resistance in nosocomial pathogens. *J Infect Dis* (2008);197 1079–81.
- [4] L.B. Rice. Progress and challenges in implementing the research on ESKAPE pathogens, *Infect. Control Hosp Epidemiol* 2010;31: 7–10.
- [5] Yanagida H, Okada M, Masuda M, Ueki M, Narama I, Kitao S, et al. Cell adhesion and tissue response to hydroxyapatite nanocrystal-coated poly(L-lactic acid) fabric. *Journal of bioscience and bioengineering* 2009;108:235-43.
- [6] Mahmoud WH, Mohamed GG, Elsaywy HA, Radwan MA. Metal complexes of novel Schiff base derived from the condensation of 2-quinoline carboxaldehyde and ambroxol drug with some transition metal ions. *Applied Organometallic Chemistry* 2018;32:e4392.
- [7] Mahmoud WH, Deghadi RG, Mohamed GG. Cyclometalated complexes containing ferrocenyl Schiff base: Preparation, characterization, DFT calculations, application in cancer and biological researches and MOE studies. *Arabian Journal of Chemistry* 2020;13:5390-405.
- [8] Zhu S, Zhai S, Chen Z, Su H, Zhang C, Liu R, et al. Cyclometalated Pt(II) complexes with tetradentate Schiff base ligands: Synthesis, photophysics, electrochemical studies and optical power limiting performance. *Dyes and Pigments* 2020;182:108591.
- [9] Mahmoud WH, Deghadi RG, Mohamed GG. Metal complexes of ferrocenyl-substituted Schiff base: Preparation, characterization, molecular structure, molecular docking studies, and biological investigation. *Journal of Organometallic Chemistry* 2020;917:121113.
- [10] Dhanaraj CJ, Jebapriya M. Metal schiff base complexes of tridentate antipyrine based ligand: Synthesis, spectral characterisation, image analysis and biological studies. *Journal of Molecular Structure* 2020;1220:128596.
- [11] Mahmoud WH, Mahmoud NF, Mohamed GG. Mixed ligand complexes of the novel nanoferrocene based Schiff base ligand (HL): Synthesis, spectroscopic characterization, MOE studies and antimicrobial/anticancer activities. *Journal of Organometallic Chemistry* 2017;848:288-301.
- [12] Abou-Hussein AA, Linert W. Synthesis, spectroscopic studies and inhibitory activity against bacteria and fungi of acyclic and macrocyclic transition metal complexes containing a triamine coumarine Schiff base ligand. *Spectrochimica acta Part A, Molecular and biomolecular spectroscopy* 2015;141:223-32.
- [13] Mahmoud W, Refaat AM, Mohamed GG. Nano Schiff base and its metal complexes: Synthesis, Characterization tools, biological applications and molecular docking studies Walaa H. Mahmouda,b\*, Ahmed M. Refaata, Gehad G. Mohameda, b a. Chemistry Department, Faculty of Science, Cairo University, Giza, 126103, Egypt b. Egypt Nanotechnology Center, Cairo University, 6th October City, Giza, El-Sheikh Zayed, 12588, Egypt. *Egyptian Journal of Chemistry* 2019;0:0-

- [14] Alghool S. Metal complexes of azo coumarin derivative: synthesis, spectroscopic, thermal, and antimicrobial studies. *Journal of Coordination Chemistry* 2010;63:3322-33.
- [15] Ilic DR, Jevtic VV, Radic GP, Arsikin K, Ristic B, Harhaji-Trajkovic L, et al. Synthesis, characterization and cytotoxicity of a new palladium(II) complex with a coumarine-derived ligand. *Eur J Med Chem* 2014;74:502-8.
- [16] <8---Applications-of-sustainable-polymer-composit\_2021\_Advances-in-Sustainabl.pdf>.
- [17] <3D-printing-of-silk-microparticle-reinforced-polycapr\_2021\_Materials-Science.pdf>.
- [18] Mahmoud WH, Mahmoud NF, Mohamed GG, El-Bindary AA, El-Sonbati AZ. Supramolecular structural, thermal properties and biological activity of 3-(2-methoxyphenoxy)propane-1,2-diol metal complexes. *Journal of Molecular Structure* 2015;1086:266-75.
- [19] Kapila A, Kaur M, Kaur H. Organotin(IV) complexes of tridentate (O,N,O) Schiff base ligand: computational, spectroscopic and biological studies. *Materials Today: Proceedings* 2020.
- [20] Bakhsheshi-Rad HR, Akbari M, Ismail AF, Aziz M, Hadisi Z, Pagan E, et al. Coating biodegradable magnesium alloys with electrospun poly-L-lactic acid- $\alpha$ -kermanite-doxycycline nanofibers for enhanced biocompatibility, antibacterial activity, and corrosion resistance. *Surface and Coatings Technology* 2019;377:124898.
- [21] R.M. Burger. Nature of Activated Bleomycin. 2000:540-46592-8\_10.
- [22] Mondal S, Nguyen TP, Pham VH, Hoang G, Manivasagan P, Kim MH, et al. Hydroxyapatite nano bioceramics optimized 3D printed poly lactic acid scaffold for bone tissue engineering application. *Ceramics International* 2020;46:3443-55.
- [23] W.A. Wani UB, S. Shreaz, . Recent advances in iron complexes as potential anticancer agents, . *New J Chem* (2016);40 1063–90.
- [24] C. Orvig MJA. Medicinal inorganic chemistry: introduction, *Chem* 1999;99:2201–3.
- [25] F. Arnesano GN. Mechanistic insight into the cellular uptake and processing of cisplatin 30 years after its approval by FDA, . *Coord Chem Rev* (2009);253:2070–81.
- [26] C. Santini MP, V. Gandin, M. Porchia, F. Tisato, C. Marzano, . Advances in copper complexes as anticancer agents, . *Chem Rev* 2014;114:815–62.
- [27] El-Sonbati AZ, El-Bindary AA, Diab MA, Abou-Dobara MI, Abdo EE. Supramolecular structure, spectroscopic, thermal studies and antimicrobial activities of Schiff base complexes. *Research on Chemical Intermediates* 2016;43:577-629.
- [28] <Energy-saving-anammox-technology-based-nitrogen-removal-a\_2021\_Renewable-and.pdf>.
- [29] Mahmoud WH, Mohamed GG, El-Dessouky MM. Coordination modes of bidentate lornoxicam drug with some transition metal ions. Synthesis, characterization and in vitro antimicrobial and antibreastic cancer activity studies. *Spectrochimica acta Part A, Molecular and biomolecular spectroscopy* 2014;122:598-608.
- [30] <A-3D-porous-fluorescent-hydrogel-based-on-amino-modified-ca\_2021\_Journal-of-.pdf>.
- [31] El Sayed Aly MR, Abd El Razek Fodah HH, Saleh SY. Antiobesity, antioxidant and cytotoxicity activities of newly synthesized chalcone derivatives and their metal complexes. *Eur J Med Chem* 2014;76:517-30.
- [32] Patil D, Wasson MK, Aravindan S, Vivekanandan P, Rao PV. Antibacterial and cytocompatibility study of modified Ti6Al4V surfaces through thermal annealing. *Materials science & engineering C, Materials for biological applications* 2019;99:1007-20.
- [33] Kumar G, Devi S, Kumar D. Synthesis of Schiff base 24-membered trivalent transition metal derivatives with their anti-inflammation and antimicrobial evaluation. *Journal of Molecular Structure* 2016;1108:680-8.
- [34] Akila E, Usharani M, Ramachandran S, Jayaseelan P, Velraj G, Rajavel R. Tetradentate-arm Schiff base derived from the condensation reaction of 3,3'-dihydroxybenzidine, glyoxal/diacetyl and 2-aminophenol: Designing, structural elucidation and properties of their binuclear metal(II) complexes. *Arabian Journal of Chemistry* 2017;10:S2950-S60.
- [35] Creaven BSD, M.Karcz, D.Kellett, A.McCann, M.Noble, A.Walsh, M. . Copper(II) complexes of coumarin-derived Schiff bases and their anti-Candida activity. *J Inorg Biochem* 2009;103:1196-203.
- [36] Al-Hyali E, Al-Abady R, rsquo, ed, Altaie F. Correlation Study for The Determination of pKa of A Number of Schiff Bases Derived from N-Formyl Pyridine using Quantum Mechanical Methods. *Egyptian Journal of Chemistry* 2020;0:0-.
- [37] Mahmoud WH, Deghadi RG, Mohamed GG. Novel Schiff base ligand and its metal complexes with some transition elements. Synthesis, spectroscopic, thermal analysis, antimicrobial and in vitro anticancer activity. *Applied Organometallic Chemistry* 2016;30:221-30.
- [38] Hussainorcid GFHFWeoMAAFSA. Synthesis, Spectroscopic characterization and bactericidal valuation of some metal (II) complexes with new Tridentate Heterocyclic Azo Ligand Type (NNO) Donor. *Egyptian Journal of Chemistry* 2021.

- [39] Hassan A, Heikal B, Khamis h, Younis A, Hassan G, Marzouk E, et al. Design, Synthesis, DFT Studies and Anticancer Activity of Novel Metal Complexes Containing 1,3,5-triazino[1,2-a]benzimidazole Moiety Using Microwave as an Approach for Green Chemistry. *Egyptian Journal of Chemistry* 2020;0:0-.
- [40] Mohamed GG, Mahmoud WH, Diab MA, El-Sonbati AZ, Abbas SY. Synthesis, characterization, theoretical study and biological activity of Schiff base nanomaterial analogues. *Journal of Molecular Structure* 2019;1181:645-59.
- [41] Zaki N, Mahmoud W, El Kerdawy A, Abdallah A, Mohamed G. Structural Characterization, Thermal Analyses, Antiproliferative and Antimicrobial Activity of Cocaine Complexes with Mn(II) and Cu(II). *Egyptian Journal of Chemistry* 2019;0:0-.
- [42] Viezzer C, Mazzuca R, Machado DC, de Camargo Forte MM, Gomez Ribelles JL. A new waterborne chitosan-based polyurethane hydrogel as a vehicle to transplant bone marrow mesenchymal cells improved wound healing of ulcers in a diabetic rat model. *Carbohydrate polymers* 2020;231:115734.
- [43] Venkataprasanna KS, Prakash J, Vignesh S, Bharath G, Venkatesan M, Banat F, et al. Fabrication of Chitosan/PVA/GO/CuO patch for potential wound healing application. *International journal of biological macromolecules* 2020;143:744-62.
- [44] Veeraperumal S, Qiu H-M, Zeng S-S, Yao W-Z, Wang B-P, Liu Y, et al. Polysaccharides from *Gracilaria lemaneiformis* promote the HaCaT keratinocytes wound healing by polarised and directional cell migration. *Carbohydrate polymers* 2020;241:116310.
- [45] Mahmoud WH, Mahmoud NF, Mohamed GG, El-Sonbati AZ, El-Bindary AA. Synthesis, spectroscopic, thermogravimetric and antimicrobial studies of mixed ligands complexes. *Journal of Molecular Structure* 2015;1095:15-25.
- [46] JEAN-PHILIP PIQUEMAL AM, CLAUDE GIESSNER-PRETTRE, OLIVIER PARISEL, . A CSOV Study of the Difference between HF and DFT Intermolecular Interaction Energy Values: The Importance of the Charge Transfer Contribution, . Wiley InterScience, 2015.
- [47] J. S. Murray K. Sen *Molecular Electrostatic Potentials, Concepts and Applications*. Elsevier, Amsterdam 1996.
- [48] F. J. Luque MO, P. K. Bhadane , S.R. Gadre , . *J Phys Chem* (1993). :9380–4
- [49] Z. Nisa AG, Z. Akhter, M.A. Nadeem, M.N. Tahir, M.U. Ahmed. *J Organometal Chem* 2016;820:130-40.
- [50] E. Üstün MÇ, M. Çelebi, Gizem, S. Demir, I. Özdemirb. . *Inorg Chim Acta* 2016;450:182-9. .
- [51] A.Y. Al-Dawood NME-M, H.A. El-Ghamry. Molecular docking and DFT studies on some nano-meter binuclear complexes derived from hydrazine-carbothioamide ligand, synthesis, thermal, kinetic and spectral characterization *J Mol Liq* 2016;220:311–23.
- [52] B. Jini kumari VAD, C. Anuba, N. S. Femila Nirmal & T. F. Abbs Fen Rej, . Molecular structure, vibrational assignment, HOMO-LUMO, Mulliken's charge analysis and DFT studies of 2-[2,4-bis(phenylamino)thiazol-5-oyl]benzothiazole. *Journal of Research in Science* December 2014;2: 55-8
- [53] I. Fleming JWaS, *New York Frontier Orbitals and Organic Chemical Reactions* 1976.
- [54] Lerner DA, Weinberg J, Cimpoesu F, Balaceanu-Stolnici C. Theoretical study of DHEA: comparative HF and DFT calculations of the electronic properties of a complex between DHEA and serotonin. *J Mol Model* 2006;12:146-51.
- [55] R. Zaky AF, Y.G. Abou El-Reash, H.M. Youssef, A.Y. Kareem. *Egy. . J Basic and App Sci*, (2016);3 272–86.
- [56] A.Y. Al-Dawood NME-M, H.A. El-Ghamry. . Molecular docking and DFT studies on some nano-meter binuclear complexes derived from hydrazine-carbothioamide ligand, synthesis, thermal, kinetic and spectral characterization *J Mol Liq* 2016;220:311–23.
- [57] M.A. Neelakantan SSM, J. Dharmaraja, T. Jeyakumar, K. Muthukumar. . *Spectrochim Acta Part A*, 2008;71:628–35. .